High temperature electrons exhausted from rf plasma sources along a magnetic nozzle

Kazunori Takahashi, , Hikaru Akahoshi, , Christine Charles, , Rod W. Boswell, and , and Akira Ando

Citation: Physics of Plasmas **24**, 084503 (2017); doi: 10.1063/1.4990110
View online: http://dx.doi.org/10.1063/1.4990110
View Table of Contents: http://aip.scitation.org/toc/php/24/8
Published by the American Institute of Physics

High temperature electrons exhausted from rf plasma sources along a magnetic nozzle

Kazunori Takahashi,[1,a)] Hikaru Akahoshi,[1] Christine Charles,[2] Rod W. Boswell,[2] and Akira Ando[1]
[1]*Department of Electrical Engineering, Tohoku University, Sendai 980-8579, Japan*
[2]*Space Plasma, Power and Propulsion Laboratory, Research School of Physics and Engineering, The Australian National University, Canberra ACT 2601, Australia*

(Received 14 June 2017; accepted 26 July 2017; published online 8 August 2017)

Two dimensional profiles of electron temperature are measured inside and downstream of a radiofrequency plasma thruster source having a magnetic nozzle and being immersed in vacuum. The temperature is estimated from the slope of the fully swept *I-V* characteristics of a Langmuir probe acquired at each spatial position and with the assumption of a Maxwellian distribution. The results show that the peripheral high temperature electrons in the magnetic nozzle originate from the upstream antenna location and are transported along the "connecting" magnetic field lines. Two-dimensional measurements of electron energy probability functions are also carried out in a second simplified laboratory device consisting of the source contiguously connected to the diffusion chamber: again the high temperature electrons are detected along the magnetic field lines intersecting the wall at the antenna location, even when the antenna location is shifted along the main axis. These results demonstrate that the peripheral energetic electrons in the magnetic nozzle mirror those created in the source tube. *Published by AIP Publishing.* [http://dx.doi.org/10.1063/1.4990110]

Plasma expansion along a magnetic nozzle (MN) is an important research topic which relates to radio frequency (rf) MN plasma thrusters.[1–7] The effect of the MN on thrust generation has been identified in helicon thruster experiments;[8,9] it originates from the Lorentz force via the radial magnetic field and the plasma-induced azimuthal electric current as predicted by some models;[8,10–12] the models and analysis detailed in Refs. 8 and 12 show that this current agrees fairly well with the electron diamagnetic drift current. Since the azimuthal current depends on the profiles of plasma density, temperature, and the electric and magnetic fields (when considering the Hall current), understanding the fine structural details of the plasma within the MN is essential.

Basic laboratory experiments have reported simultaneous formations of a conical density structure and peripheral high energy electrons downstream of the plasma source along the last magnetic field line intersecting the wall of the source open exit, i.e., the surface of the MN.[13–15] Earlier experimental work on the electron energy probability function (EEPF) discussed the transport of the high temperature electrons from the source to the diffusion chamber, based on measurements performed at two discrete axial positions inside and downstream of the source.[14] A two-dimensional (2D) density mapping has suggested the possibility of additional ionization by the energetic electrons in the diffusion chamber,[15] and heating of the electrons by the skin effect near the antenna in the source has also been discussed.[16,17] A particle-in-cell simulation by Singh and Rao has shown the peripheral energetic electrons at the plasma-vacuum boundary along the MN even when injecting a plasma having a uniform electron temperature;[18] these numerical studies have invoked electron heating caused by plasma instability.[19] Subsequently performed 2D measurements of the plasma density and potential have claimed that the steady-state profiles are consistent with the PIC simulation,[20] where a Lorentz force due to the azimuthal Hall current and the applied magnetic field induces a radially outward plasma transport and the resultant conical plasma structure. The effect of electron rotation due to $\nabla \mathbf{B}$ drift on confinement of electrons and resultant ionization collisions downstream of the source have also been discussed.[21] More recently, the sole measurement of the tail electrons by a retarding field energy analyzer has also been performed downstream of the source.[22] Although the presence of the peripheral energetic electrons in the MN has been observed in these numerous laboratory and numerical experiments mentioned above, its origin remains unclear because of the lack of experimental data smoothly connecting the upstream and downstream part of the source/nozzle.

Here, 2D measurements of the electron temperature are performed over the axial region including both the inside and the downstream side of the source to provide data continuously connecting the two regions. The experiments are carried out in two different device configurations, consisting of a source immersed in vacuum and a source attached to a diffusion chamber, respectively.

Figure 1 shows the schematic of (a) the experimental setup and (b) the axial profile of the magnetic field, as described previously.[9] The source immersed in a 60-cm-diameter and 140-cm-long vacuum chamber consists of a 6.4-cm-inner-diameter and 20-cm-long Pyrex glass tube surrounded by a double-turn rf loop antenna ($z = -11.5$ cm), where $z = 0$ corresponds to the open source exit. A solenoid creating the expanding magnetic field shown in Fig. 1(b) is

[a)]kazunori@ecei.tohoku.ac.jp

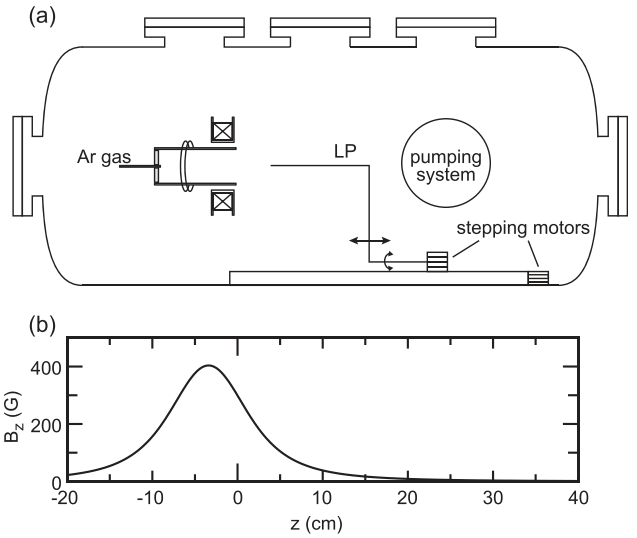

FIG. 1. (a) Schematic of the experimental setup for the source immersed in the vacuum chamber. (b) Axial profile of the magnetic field strength.

centered at $z = -3.5$ cm, where the maximum field strength is about 400 G. Argon gas is introduced from the terminating upstream side of the source with a gas flow rate of 24 sccm giving a chamber pressure of about 0.8 mTorr. The rf antenna is powered by a 13.56 MHz and 1 kW rf generator via a vacuum feedthrough and an impedance matching circuit located outside the chamber. Excessive thermal load prevented the use of an rf compensated probe (which includes LC resonant inductors) in the source. Therefore, an uncompensated planar Langmuir probe facing radially is mounted on a movable motor stage; a probe bias voltage is swept between ± 100 V and the electron temperature is estimated from the slope of the semi-logarithmic plot of the *I–V* characteristics at each measurement position. The plasma density is estimated from the measured ion saturation current and the electron temperature. The local plasma potential corresponds to the peak of the first derivative of the *I–V* characteristics.

Figure 2 shows the colour contour plots of the measured 2D (r–z) profiles of the electron temperature T_e [Fig. 2(a)], the logarithm of the plasma density $\log(n_p)$ [Fig. 2(b)], and the plasma potential V_p [Fig. 2(c)] together with the magnetic field lines. The radial profiles of T_e (crosses) and n_p (open squares) measured at $z = 6$ cm are shown in Fig. 2(d). The high electron temperature region exists between the second and third magnetic field lines from the centre over the continuous axial regions from $z \sim -15$ to $z \sim 20$ cm as seen in Fig. 2(a): the high temperature electrons are generated near the rf antenna at $z \sim -11$ cm and transported along the expanding magnetic field lines. Around these magnetic field lines downstream of the source exit, a slightly high density region is detected (open squares for n_p in Fig. 2(d) peaking at $r \sim \pm 4$ cm), which seems to be a result of enhanced local ionization by the high electron temperature since T_e is also peaking at $r \sim \pm 4$ cm [Fig. 2(d)]. Nevertheless, the U-shaped plasma potential structure having a maximum on axis is observed in Fig. 2(c) and in agreement with previous measurements in similar devices.[23,24]

Here, the measurements in Fig. 2 are performed with the uncompensated Langmuir probe and the assumption of a

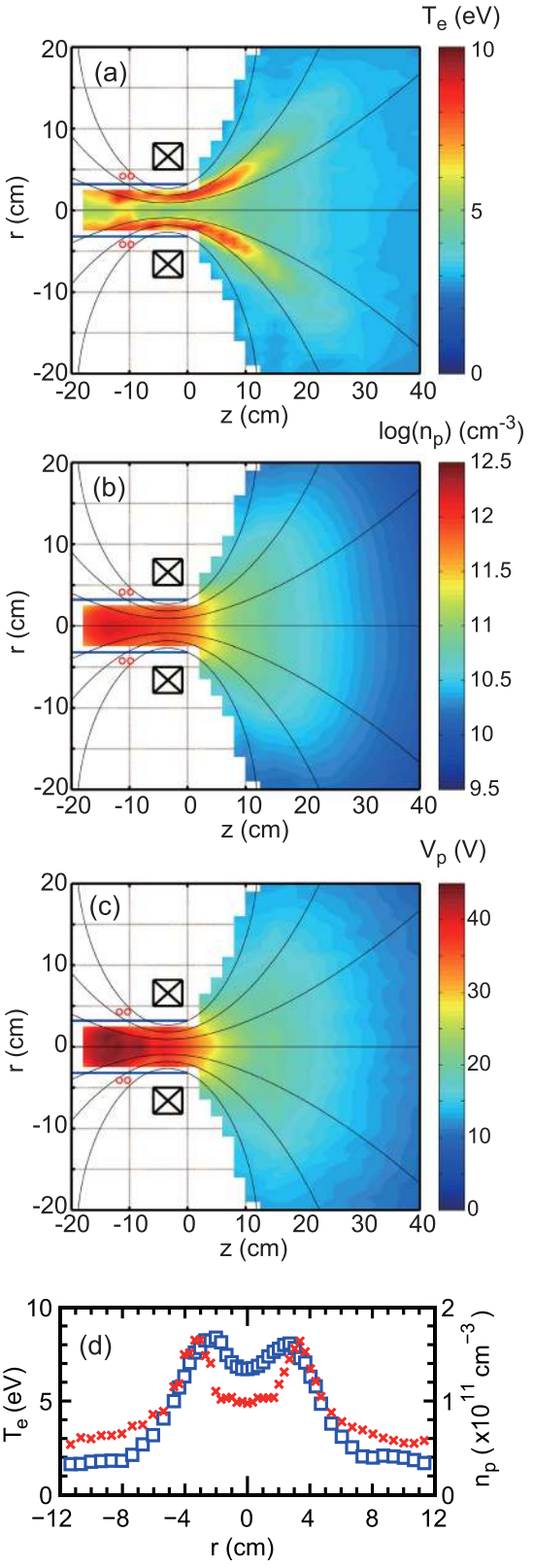

FIG. 2. 2D profiles of (a) the electron temperature T_e, (b) the logarithm of the plasma density $\log(n_p)$, and (c) the plasma potential V_p measured for the setup in Fig. 1. (d) Radial profiles of T_e (crosses) and n_p (open squares) measured at $z = 6$ cm, where the data are extracted from Figs. 2(a) and 2(b).

Maxwellian distribution for the analysis, whereas the previous experiments have shown a non-Maxwellian distribution in the similar setup.[14] To gain more confidence on the presence of the high temperature electrons over the axial region

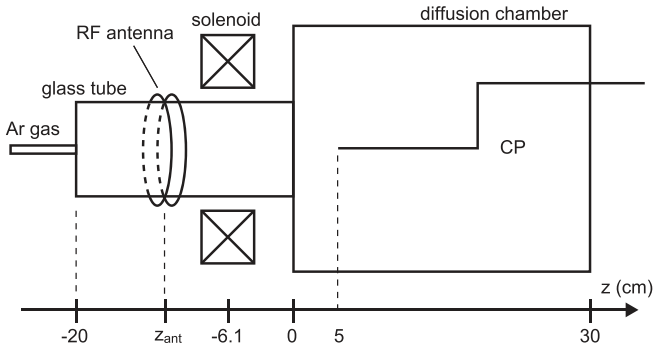

FIG. 3. Schematic of the experimental setup for the source attached to the diffusion chamber.

including both the inside and the downstream side of the source, EEPF measurements are performed using a more basic laboratory device shown in Fig. 3, which also allows for the antenna location to be easily modified. The device has a 9.5-cm-diameter and 20-cm-long Pyrex source tube connected to a 26-cm-diameter and 30-cm-long grounded diffusion chamber. A solenoid centred at $z = -6.1$ cm provides a peak magnetic field strength of about 200 G decreasing to ~25 G at $z = 10$ cm. The axial position of the double-turn rf antenna is defined as z_{ant}; two different antenna positions of $z_{ant} = -12.5$ and –16.5 cm are tested here. Argon gas pressure in the diffusion chamber is maintained at 1.5 mTorr; the 13.56 MHz and 400 W rf power signal is continuously supplied to the antenna. The measurement of the EEPF is performed by combining an rf-compensated Langmuir probe following Ref. 25 and an analogue differentiation technique,[26] as described previously.[27]

Typical EEPFs measured at $(z, r) = (5\,\text{cm}, 0\,\text{cm})$ and $(5\,\text{cm}, 6\,\text{cm})$ are plotted as solid and dotted lines, respectively, in Fig. 4. The value of the EEPF at $r = 6$ cm is found to be greater than that measured at $r = 0$ for energies above ~15 eV, which implies that the averaged electron energy at $r = 6$ cm is higher than that at $r = 0$. The effective electron temperature T_{eff} is obtained by integrating the measured EEPF as described in Ref. 28.

2D profiles of T_{eff} measured for the two distinct antenna positions of $z_{ant} = -12.5$ cm and –16.5 cm are shown in Figs. 5(a) and 5(b), respectively, together with the magnetic field lines (dashed lines), where the bold solid lines are the physical boundaries of the source and the chamber. The high electron temperature is continuously observed in both Figs. 5(a) and 5(b) when probing from the inside to the downstream side of the source along the expanding magnetic field lines, similar to the result shown in Fig. 2(a). The high temperature region in Fig. 5(a) seems to cover an outer region

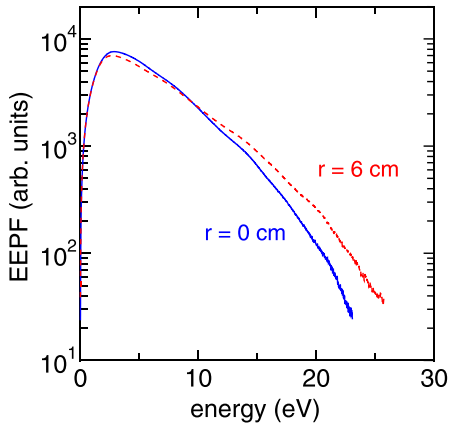

FIG. 4. Typical EEPFs measured at $(z, r) = (5\,\text{cm}, 0\,\text{cm})$ (solid line) and $(5\,\text{cm}, 6\,\text{cm})$ (dotted line) for the setup in Fig. 3, with the antenna position set at $z_{ant} = -12.5$ cm.

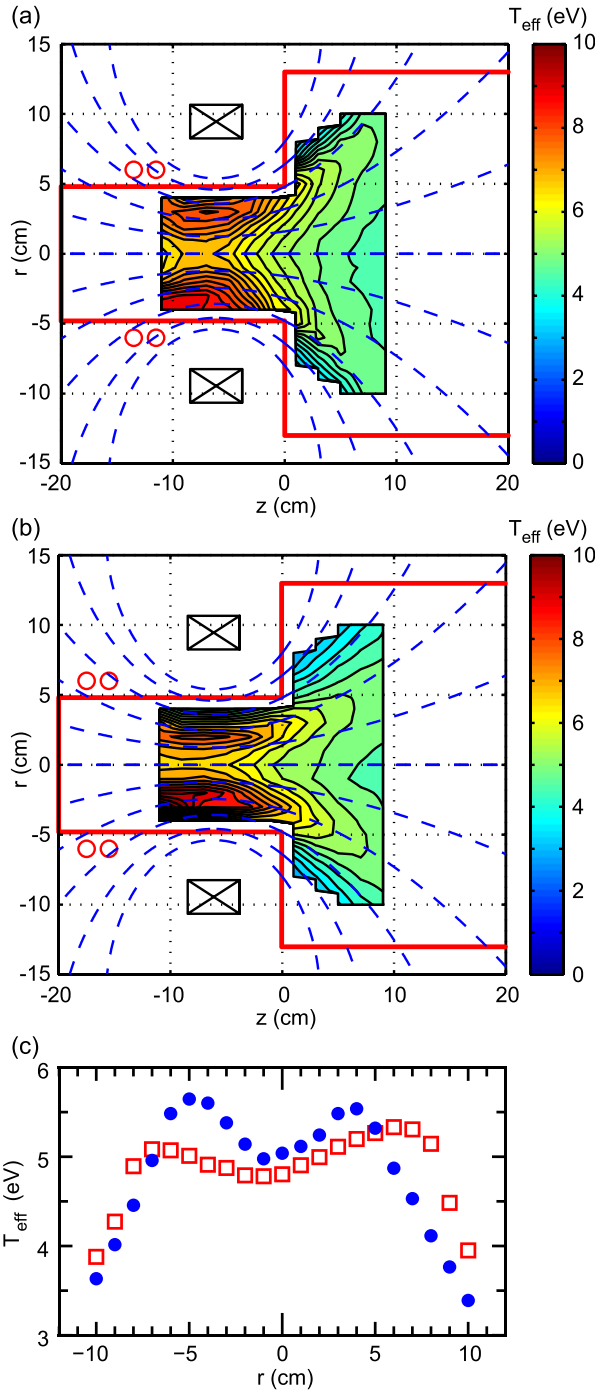

FIG. 5. 2D profiles of T_{eff} measured for the setup in Fig. 3, where the antenna position is set to values of (a) $z_{ant} = -12.5$ cm and (b) $z_{ant} = -16.5$ cm, respectively, as indicated by the open circles. The dashed lines are the applied magnetic field lines. (c) Radial profiles of T_{eff} at $z = 5$ cm for $z_{ant} = -12.5$ cm (open squares) and $z_{ant} = -16.5$ cm (filled squares), where the data are extracted from Figs. 5(a) and 5(b).

extending radially a bit more than seen in Fig. 5(b) and again follows the magnetic field lines intersecting the wall near the antenna. To look at the profile in more detail, the radial profiles of T_{eff} at $z = 5$ cm are plotted in Fig. 5(c) as open squares and filled circles for the $z_{ant} = -12.5$ cm and $z_{ant} = -16.5$ cm cases, respectively. When the antenna is shifted upstream, the radial location of the peak in temperature is shifted to the radially inward direction since the magnetic field line intersecting the wall at the rf antenna position traverses a more central region of the diffusion chamber. Hence, electron heating by the antenna, where the power is transferred to the electrons via the skin effect,[17] seems to be the main contribution to the presence of the high temperature electrons near the source wall with subsequent transport along the field lines into the diffusion chamber. It should be mentioned that the trapping length of the electrons also affects the electron temperature as presented in previous numerical work.[29] This possible additional contribution to the formation of the peripheral high temperature electrons in the source is the subject of future investigation.

In summary, 2D measurements of the electron temperature have been performed in magnetically expanding plasmas under various configurations. Two interpretations regarding the presence of high temperature electrons near the plasma-vacuum boundary in the MN have been discussed over the last few years; one is the leakage of the high energy electrons created by the skin heating in the source and the other is electron heating by plasma instability in the MN. The present results demonstrated by taking data contiguously connecting the upstream and downstream regions in two different devices clearly show that the first interpretation is the main contribution to the formation of the peripheral high electron temperature in the MN.

Regarding the conical density profiles observed in the MN, it has been proposed that the radially outward $\mathbf{J} \times \mathbf{B}$ force due to the electron Hall current ($\mathbf{E} \times \mathbf{B}$ drift current) is responsible for the structure formation,[18] in addition to additional ionization in the diffusion chamber. However, the measured azimuthal current in the helicon thruster is essentially diamagnetic near the source exit,[30] i.e., in the opposite direction to the Hall current. Therefore, further investigation is still required for a complete understanding of the dynamics and structure formation in magnetically expanding plasmas.

This work was partially supported by grants-in-aid for scientific research (16H04084 and 26247096) from the Japan Society for the Promotion of Science.

[1]B. W. Longmier, L. D. Cassady, M. G. Ballenger, M. D. Carter, F. R. Chang-Díaz, T. W. Glover, A. V. Ilin, G. E. McCaskill, C. S. Olsen, and J. P. Squire, J. Propul. Power **27**, 915 (2011).
[2]F. Cannat, T. Lafleur, J. Jarrige, P. Chabert, P.-Q. Elias, and D. Packan, Phys. Plasmas **22**, 053503 (2015).
[3]C. Charles, J. Phys. D: Appl. Phys. **42**, 163001 (2009) and references therein.
[4]L. T. Williams and M. L. R. Walker, J. Propul. Power **29**, 520 (2013).
[5]T. Harle, S. J. Pottinger, and V. J. Lappas, Plasma Sources Sci. Technol. **22**, 015015 (2013).
[6]K. Takahashi, A. Komuro, and A. Ando, Plasma Sources Sci. Technol. **24**, 055004 (2015).
[7]D. Kuwahara, S. Shinohara, and K. Yano, J. Propul. Power. **33**, 420 (2017).
[8]K. Takahashi, T. Lafleur, C. Charles, P. Alexander, and R. W. Boswell, Phys. Rev. Lett. **107**, 235001 (2011).
[9]K. Takahashi, C. Charles, and R. W. Boswell, Phys. Rev. Lett. **110**, 195003 (2013).
[10]A. Fruchtman, Phys. Rev. Lett. **96**, 065002 (2006).
[11]E. Ahedo and M. Merino, Phys. Plasmas **17**, 073501 (2010).
[12]A. Fruchtman, K. Takahashi, C. Charles, and R. W. Boswell, Phys. Plasmas **19**, 033507 (2012).
[13]W. Cox, R. Hawkins, C. Charles, and R. Boswell, IEEE Trans. Plasma Sci. **36**, 1386 (2008).
[14]K. Takahashi, C. Charles, R. Boswell, W. Cox, and R. Hatakeyama, Appl. Phys. Lett. **94**, 191503 (2009).
[15]C. Charles, Appl. Phys. Lett. **96**, 051502 (2010).
[16]Y. Zhang, C. Charles, and R. Boswell, Phys. Plasmas **23**, 083515 (2016).
[17]Y. Zhang, C. Charles, and R. Boswell, J. Phys. D: Appl. Phys. **50**, 015205 (2017).
[18]S. Rao and N. Singh, Phys. Plasmas **19**, 093507 (2012).
[19]N. Singh, S. Rao, and P. Ranganath, Phys. Plasmas **20**, 032111 (2013).
[20]S. K. Saha, S. Chowdhury, M. S. Janaki, A. Ghosh, A. K. Hui, and S. Raychaudhuri, Phys. Plasmas **21**, 043502 (2014).
[21]S. Ghosh, S. Yadav, K. K. Barada, P. K. Chattopadhyay, J. Ghosh, R. Pal, and D. Bora, Phys. Plasmas **24**, 020703 (2017).
[22]N. Gulbrandsen and Å. Fredriksen, Front. Phys. **5**, 2 (2017).
[23]C. Charles, R. W. Boswell, and R. Hawkins, Phys. Rev. Lett. **103**, 095001 (2009).
[24]K. Takahashi, Y. Igarashi, and T. Fujiwara, Appl. Phys. Lett. **97**, 041501 (2010).
[25]I. D. Sudit and F. F. Chen, Plasma Sources Sci. Technol. **3**, 162 (1994).
[26]K. F. Schoenberg, Rev. Sci. Instrum. **49**, 1377 (1978).
[27]K. Takahashi, C. Charles, R. Boswell, M. A. Lieberman, and R. Hatakeyama, J. Phys. D: Appl. Phys. **43**, 162001 (2010).
[28]K. Takahashi, C. Charles, R. W. Boswell, and T. Fujiwara, Phys. Rev. Lett. **107**, 035002 (2011).
[29]R. Boswell, C. Charles, and K. Takahashi, Bull. Am. Phys. Soc. **56**, BAPS.2011.GEC.AM1.13 (2011).
[30]K. Takahashi, A. Chiba, A. Komuro, and A. Ando, Plasma Sources Sci. Technol. **25**, 055011 (2016).